

Patterns, Forces and Metastable Pathways in Debonding of Elastic Films

Jayati Sarkar¹, Vijay Shenoy^{2,*} and Ashutosh Sharma^{1†}

¹ *Chemical Engineering Department, Indian Institute of Technology Kanpur, UP 208 016, India*

² *Material Research Centre, Indian Institute of Science, Bangalore 560 012, India*

The letter resolves several intriguing and fundamental aspects of debonding at soft interfaces, including the formation and persistence of regularly arranged nanocavities and bridges, “adhesion-debonding hysteresis”, and vastly lower adhesive strengths compared to the absence of pattern formation. The analysis shows the hysteresis to be caused by an energy barrier that separates the metastable patterned configurations during withdrawal, and the debonded state. The metastable morphological pathways involving cavitation and peeling of contact zones engender substantially lower debonding forces.

PACS numbers: 82.35.Gh, 68.35.Ct, 68.55.-a, 46.50.+a

The related phenomena of adhesion, debonding and interfacial cavitation or cracking at soft elastic interfaces have been intensely studied both in view of their technological applications and the many unresolved scientific issues related to the pathways, morphology and forces of debonding. A rigid surface (contactor) initially in contact with a soft elastic film, upon withdrawal, debonds by the formation of a pattern of well defined spacing consisting of areas of intimate contact and interfacial cavities [1, 2, 3, 4]. A linear stability analysis [5] showed spontaneous surface roughening of the film when the contactor is initially brought in close proximity ($< 20\text{nm}$). The wavelength (λ) of this surface pattern depends only on the film thickness (h) ($\lambda \sim 3h$), but is independent of the strength and nature of the adhesive interactions as well as the elastic properties of the film. The regions of adhesive contact persist until the contactor is pulled to a much larger distance than that at which the initial contact instability was triggered upon approach. This difference between approach and withdrawal behaviors may be referred to as “adhesion-debonding or contact hysteresis”. Another interesting aspect is the pull-off force required for debonding can be several orders smaller than the force calculated based on the assumption of flat surfaces. Clearly, such a significant reduction cannot be explained merely by $\sim 50\%$ reduction in the contact area observed at detachment [3]. The mechanism of “adhesion-debonding hysteresis”, its associated morphologies including patterned cavitation, pull-off force and distance are the key unresolved issues in debonding at soft interfaces that are addressed here.

Figure. 1 illustrates the film-contactor geometry. The total energy consists of the stabilizing stored elastic energy and the destabilizing attractive interaction between the contactor and the film.

$$\Pi = \int_V W(\epsilon) dV + \int_S U(d_0 - \mathbf{u} \cdot \mathbf{n}) dS, \quad (1)$$

where W is the strain energy density defined as, $W(\epsilon) = \frac{1}{2}\mu(\epsilon : \epsilon)$ with ϵ is the strain tensor, \mathbf{u} is the displacement vector, μ is the shear modulus of the film

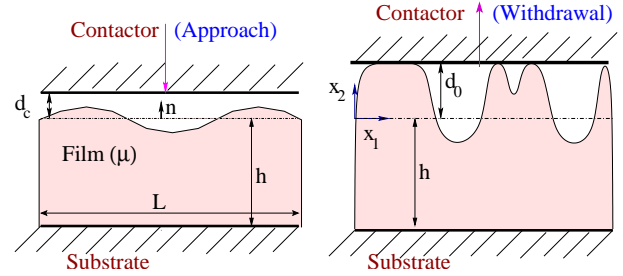


FIG. 1: Left: Schematic of small amplitude pattern formation on approach at critical distance d_c . Right: Column stretching and growth of cavities on withdrawal of the contactor.

($\lesssim 10\text{MPa}$). The interaction potential consists of an attractive van der Waals component along with a short range Born repulsion, represented by $U(d_0 - \mathbf{u} \cdot \mathbf{n}) = -A/12\pi(d_0 - \mathbf{u} \cdot \mathbf{n})^2 + B/(d_0 - \mathbf{u} \cdot \mathbf{n})^8$ where A is the Hamaker constant (of the order of 10^{-20}J) and B is the coefficient of Born repulsion. The coefficient B is correlated to the adhesive energy at contact ($\Delta G = U(d_e) = A/(16\pi d_e^2)$), where d_e is the equilibrium separation distance obtained from $U'(d_e) = 0$. This form of interaction implies that the force required to pull off two rigid flat surfaces is $F_{max}^{flat} = \Delta G/d_e$. As may be expected, our detailed studies (to be published) have confirmed that the debonding is controlled by the adhesive energy rather than the detailed functional form of the potential. Based on the linear stability of eqn. (1), it was shown that the film surface becomes spontaneously rough as the contactor approaches it to within a small critical distance d_c at which $h|U''|/\mu \geq 6.22$. The lengthscale of the pattern consisting of cavities and bridges (regions of contact) is about three times the film thickness regardless of the interaction potential and the elastic properties; both of which are in agreement with observations [2, 3, 4].

We explain the physical basis of the adhesion-debonding hysteresis (debonding distance $\gg d_c$) by the following simple analysis which is also in conformity with the detailed simulations presented here. For

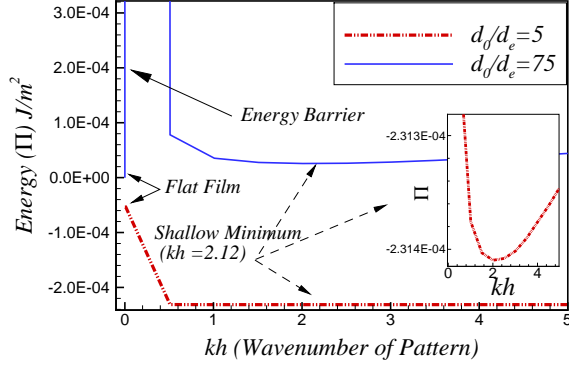


FIG. 2: Energy landscape as a function of wavenumber. The plots show the presence of an energy barrier separating the flat film and patterned state for large values of d_0/d_e . The physical parameters are $\mu = 0.1\text{MPa}$, $h = 10\text{microns}$, $A = 10^{-20}\text{J}$, $\Delta G = 1.0\text{mJ/m}^2$.

a single Fourier mode, $u_2(x) = a_k \cos kx$, the total energy (per unit length of the film) is shown in fig. 2 for two different values of the gap-thickness d_0 above and below the critical distance d_c . As predicted by the linear stability, the patterned configuration with $hk \approx 2.12$ ($\lambda \sim 3h$) has the lowest energy for $d_0 < d_c$ rather than flat film. However, for $d_0 > d_c$, the flat film configuration has the lower energy, although the patterned state remains a *local* minimum, metastable state. For $d_0 > d_c$, the global (flat film) and the local (patterned state) minima are separated by a large energy barrier (fig. 2). *It is due to the presence this energy barrier that the patterned states formed during the approach persists in its metastable configuration upon withdrawal.* Of course, as shown by simulations, the pattern is far more complex in that it consists of many Fourier modes, leading to a multiplicity of metastable states of varying energies. Thus, during the pull off, the system “hops” through a succession of metastable states leading to a strong “path dependence” especially in the presence of heterogeneities, noise etc.

The complete simulation of the pull-off process is achieved by the Fourier representation $u_2(x_1, 0) = \sum_{n=0}^{N-1} a_n \cos(k_n x_1)$, where a_n is the amplitude of the n -th Fourier mode with wavenumber $k_n (= 2\pi n/L)$. The total energy per unit depth of the film

$$\begin{aligned} \Pi(a_1, \dots, a_n) = & \frac{\pi\mu L}{2} \sum_{n=0}^{N-1} n a_n^2 k_n S(k_n h) \\ & + \int_0^L U(d_0 - \sum_{n=0}^{N-1} a_n \cos(k_n x_1)) dx_1. \end{aligned} \quad (2)$$

The stresses that develop in the film are determined from the Fourier coefficients as $\sigma_{22}(x_1, 0) = 2\mu \sum_{n=0}^{N-1} a_n k_n S(k_n h) \cos k_n x_1$, where $S(\xi) = \frac{1 + \cosh(2\xi) + 2\xi^2}{\sinh(2\xi) - 2\xi}$. F is the average force per unit

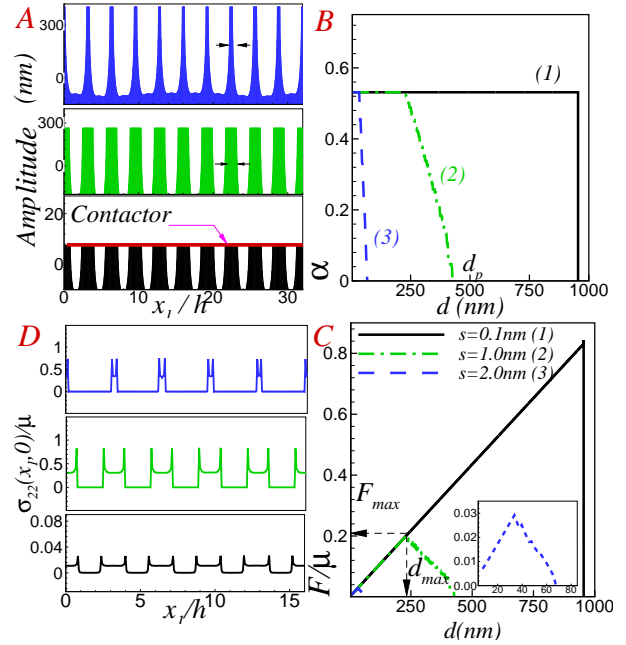


FIG. 3: (A) Film profiles at various separation distances without external noise and step size of 1nm ($A = 10^{-20}\text{J}$, $\mu = 0.5\text{MPa}$, $h = 10\text{microns}$) (B) & (C) Variation, respectively, of fractional contact area α and force F/μ with separation distances: Curves (1), (2) and (3) correspond to the step size of 0.1nm, 1nm and 2nm, respectively. Curves (1) and (3) correspond to the catastrophic column collapse and continuous peeling modes of failure, and curve (2) is an intermediate. (D) Normal stress distribution along the surface of the film for cases in (A) showing maximum stresses, responsible for peeling, at the column edges.

area exerted on the contactor plate to hold the film in equilibrium at a given separation.

A conjugate gradient(CG) scheme (which finds the local minimum closest to the initial configuration) was employed to find the Fourier coefficients that result in a minimum energy pattern for a given separation distance $d_0 > d_c$ starting from the contact proximity. The robustness of the energy minimum thus isolated was confirmed by small random perturbations of the equilibrium profile. The separation distance was increased in steps of s , taking the energy minimizing pattern of the previous step as the initial state in the CG scheme. To uncover the range of possible metastable pathways, we varied the step size s and, in addition, have considered cases where the energy minimizing Fourier coefficients (at d_0) are perturbed randomly before being taken as initial choices for the next step. The perturbations are introduced by multiplying each Fourier coefficient with $(1+r)$ where r is a random number between $-\epsilon$ and ϵ , where ϵ is called the noise amplitude.

Fig. 3A depicts typical changes in the film morphology during the process of pull off starting from the critical distance d_c where the instability originates. This fully nonlinear simulation (without any imposed

noise) shows the columns/cavities being laterally separated by $\sim 3h$ at all separation distances until the maximum force is reached. Thus, the initial contact ($d < d_c$) nanocavities predicted by the linear theory persist during pulloff. Figs. 3B and 3C show, respectively, the variation of contact area ($\alpha = \text{area of contacts}/\text{total film surface area}$) and the force F on the contactor, with gap thickness for different step sizes, 0.1nm, 1.0nm and 2.nm. For small step sizes ($\lesssim 0.1\text{nm}$) the debonding pathway is such that the configuration is trapped in the energy minimum corresponding to the initial instability. The contact area remains constant and the force increases almost linearly until a catastrophic snap-off of the bridging columns. Remarkably, the maximum force F_{max} that can be sustained before debonding is about an order of magnitude smaller than the maximum adhesive force F_{max}^{flat} . Clearly, debonding does not occur by a uniform detachment of the contacts, but rather by a different pathway, requiring much smaller pull off force, made possible by the initial pattern formation. The formation of bridges and cavities allows very high concentration of elastic stresses near the edges of the columns. For small step sizes, the elastic stresses build up to very high levels comparable to the maximum adhesive force, without any intermediate small relaxations, since the structure is trapped in the original deep energy minimum. This engenders a catastrophic adhesive failure for small step sizes. In contrast, larger step sizes force the structure to hop through a succession of metastable states with lower barrier heights releasing energy intermittently leading to a continuous decrease in the contact area. The stresses at the edges of the contacts are not large enough to cause catastrophic detachment, but are sufficient to sustain peeling. For intermediate step sizes (curve (2) of fig. 3B), the initial phase of pulling reproduces the features of small step size results, followed by the large step size behavior. The escape from the initial high barrier state occurs only after after some stretching of columns leading the release of pent-up elastic energy. The ascending branch (“elastic branch”) of the force curve Fig. 3(C) reflects the linear increase of elastic stresses in the columns without any change in the contact area. The initiation of peeling limits the maximum force, after which it declines (“release branch”) with further increase in the separation distance and a concurrent reduction in the contact area. The release branch of the force curve is realizable only in displacement controlled experiments.

A particularly simple model, which shows the essential physics of the linear decrease of the area, approximates the total energy as $\frac{3}{2}\mu u^2(\alpha/(1-\alpha)h) + \alpha U(d_0 - u)$ where α is the fractional contact area. For a given d_0 , the minimum of energy occurs when the fractional contact area is $\alpha(d_0) \approx 1 - (3\mu/2h|U(d_e)|)^{1/2} d_0$. This linear decrease in the contact area with increased separation shows that debonding, even by the application

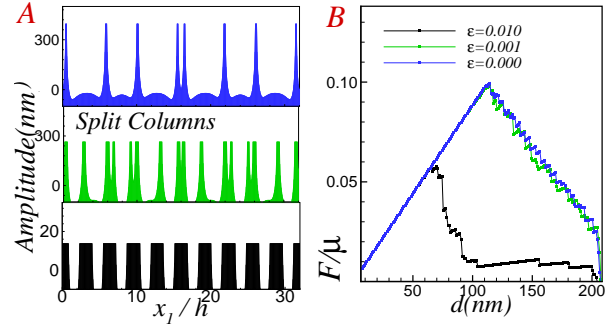


FIG. 4: (A) Noise-induced, column-splitting pathway of adhesive failure for a more strongly adherent film (same as fig. 3 except, $A = 10^{-19}\text{J}$ and $\epsilon = 0.01$) (B) Variation of force F/μ with separation distances for various levels of noise ($\epsilon = 0.0, 0.001, 0.01$).

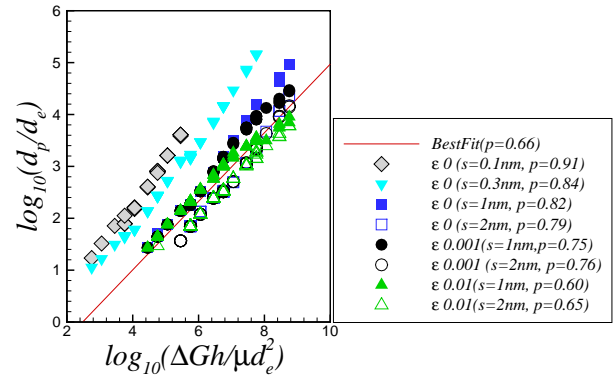


FIG. 5: Variation of snap-off distance with non-dimensional stiffness ratio. The slope of each curve is represented by p .

of a purely normal force, actually proceeds by *peeling of the contacts*. Peeling from the contact edges requires much smaller energy penalty (and force) as compared to homogeneous debonding of flat contact areas.

Although the peeling mode remains the dominant mode of debonding for small levels of noise, another pathway of debonding in the form of cavitation within the contact area leading to column splitting also appears for high noise amplitudes (fig. 4A), i. e., starting from initial conditions that are far from the solution branch being followed in the absence of noise. The column splitting mode is favored for higher adhesive strength and for more compliant films (higher value of $\Delta Gh/\mu$) where even smaller amounts of noise can induce this transition. Column splitting, when it occurs, results in precipitous decrease in the force, usually followed by a regime of more nearly constant force (fig. 4B). Continuous peeling from the sides of the split columns prevents the build-up of elastic force in the constant force regime. This helps understand experimental observations of constant force regime which becomes more prominent on rough surfaces that allow cavity initiation within the contact zones [3, 6].

The maximum pull-off distance was obtained for a

wide range of parameters $h \sim 0.1 - 50 \mu\text{m}$, $A \sim 10^{-19} - 10^{-21} J$ and $\mu \sim 0.1 - 10 \text{MPa}$, step sizes ($s \sim 0.1 - 2.0 \text{nm}$), noise amplitude ($\epsilon \sim 0.001 - 0.01$) and $\Delta G \sim 1 - 100 \text{mJ/m}^2$. Interestingly, the dependence of the pulloff distance d_p on ΔG , μ and h is represented by a master curve of the form (fig. 5)

$$\frac{d_p}{d_e} \sim \left(\frac{\Delta Gh}{\mu d_e^2} \right)^p \quad (3)$$

where the nondimensional parameter $(\Delta G/d_e^2)/(\mu/h)$ is the ratio of the stiffness of the interaction potential and the elastic stiffness of the film. The exponent p is close to 1 for noiseless cases with small step size and decreases with increasing step size as well as increasing level of noise (the minimum exponent is about 0.6). As argued earlier, increased step size and noise levels can induce debonding at smaller distance by cascading through higher energy metastable states.

Further, the maximum force from simulations was found to scale as

$$\frac{F_{max}}{\mu} = C \left(\frac{h}{d_e} \right)^\gamma \left(\frac{\Delta Gh}{\mu d_e^2} \right)^\delta \quad (4)$$

where exponents γ, δ are -0.63 and 0.24 , respectively for noiseless case with small step size ($s = 0.1 \text{nm}$), and the prefactor $C = 38.5$. In this case, $F_{max} \sim (\Delta G)^{0.25} h^{-0.4} \mu^{0.75}$. In all other cases of higher step size and noise considered, γ is found to be remarkably constant at -1 ± 0.01 and the exponent δ is 0.8 ± 0.18 . The prefactor for these exponents is in the range of 0.01 to 0.1. The force in this case scales as $F_{max} \sim (\Delta G)^{0.8} h^{-0.2} \mu^{0.2}$ showing a stronger dependence on adhesive energy but a weaker dependence on film thickness and shear modulus compared to the noiseless and small step size case. The above considerations (fig. 5) also explain the long debated contention that the surface energy of soft solids as measured from debonding experiments is a non-equilibrium and non-unique property.

The values of the maximum force per unit area required for debonding are much smaller than predicted for debonding for flat surfaces ($F_{max}^{flat} \sim \Delta G/d_e$). For example with $A = 10^{-20} J$, $h = 10.0 \mu\text{m}$, $\mu = 0.5 \text{MPa}$, $F_{max}^{flat} = 80 \text{MPa}$, $F_{max} = 0.1 \text{MPa}$ for step size 1nm without noise and $F_{max} = 0.04 \text{MPa}$ with noise. The ratio, $F_{max}/F_{max}^{flat} \sim (\mu d_e^2/\Delta Gh)^n (h/d_e)^m$, ($n > m$), where n is close to 0.2 and m close to 0 for cases with noise and relatively large steps. This shows the discrepancy in the forces between the flat and instability controlled modes of failure increases with decreasing shear modulus, increasing adhesive strength and film thickness.

Representative 2D simulations (such as shown in fig. 6) also confirm the underlying physics and the other results reported here. A detailed account will be published elsewhere.

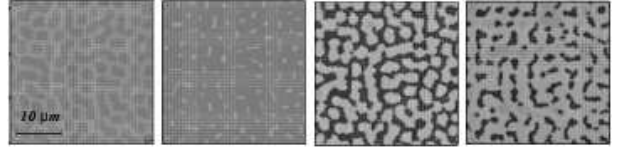


FIG. 6: The first two frames represent the instability pattern during approach ($d_0 = 5.72 \text{nm}$ and 1.43nm) and the last two represent pattern evolution during withdrawal ($d_0 = 35.43 \text{nm}$ and 43.43nm). The darker regions are the contact zones and the lighter shades denote the cavities formed within the film. During the approach a labyrinth pattern is transformed into isolated nanocavities which upon pulloff grow and fragment the contact zones. The wavelength of the pattern ($\sim 3h$) also agrees with linear theory and experimental observations [2, 3, 4].

This letter resolves important open questions regarding the mechanisms and pathways of debonding at soft interfaces. The main results include, (a) the physical origins of the adhesion-debonding hysteresis, (b) formation and persistence of regularly arranged cavities and bridges during debonding, (c) metastable pathways of debonding such as column collapse, column peeling and column splitting that require much larger pulloff distances and much smaller debonding forces as compared to detachment of flat surfaces, (d) complete quantitative dependence of pull-off distance and force on adhesion energy, shear modulus and film thickness. Formation of cavities engenders extremely high stresses near the column edges leading to the peeling of contact zones at much smaller average stresses than the adhesive strength. This is analogous to defects (dislocations and cracks) in solids which give rise to observed yield stress and strength much smaller than ideal values.

Discussions with M.K. Chaudhury and A. Ghatak are gratefully acknowledged. V. S. and A. S. acknowledge financial support of DST, India through the Nanoscience program.

* shenoy@mrc.iisc.ernet.in

† ashutos@iitk.ac.in

- [1] Y. Y. Lin, C. -Y. Hui and H. D. Conway, *J. Poly. Sci. Part B: Poly. Phys.*, **38**, 2769 (2000); C. Creton, J. Hooker, and K. R. Shull, *Langmuir*, **17**, 4948-4954 (2001).
- [2] A. Ghatak, M. K. Chaudhury, V. Shenoy and A. Sharma, *Phys. Rev. Lett.*, **85**, 4329 (2000); A. Ghatak and M. K. Chaudhury, *Langmuir*, **19**, 2621 (2003).
- [3] K. R. Shull, C. M. Flanigan and A. J. Crosby, *Phys. Rev. Lett.*, **84**, 3057 (2000); R. E. Webber, K. R. Shull, A. Roos, and C. Creton, *Phys. Rev. E.*, **68**(2), 021805 (2003).
- [4] W. Mönch, and S. Herminghaus, *Euro. Lett.*, **53**, 525 (2001).
- [5] V. Shenoy and A. Sharma, *Phys. Rev. Lett.*, **86**, 119 (2001); *J. Mech. and Phy. of Sol.*, **50**, 1155 (2002); J.

Sarkar, V. Shenoy and A. Sharma, *Phy Rev E*, **67**, 031607 (2003)., C. Q. Ru, *J. Appl. Phys.*, **90**, 6098 (2001).

[6] A. Chiche, P. Pareige and C. Creton, *C. R. Acad, Sci IV -Phys* **1** (9), 1197 (2000).